15

Coupling efficiency of single mode fiber with photonic integrated circuit based on Si_3N_4

© *I.V. Ivashentseva, I.V. Tretyakov, N.S. Kaurova, A.D. Golikov, G.N. Goltsman*

Moscow Pedagogical State University,
Moscow, Russia

e-mail: irinivas22@yandex.ru

Received August 28, 2024
Revised October 02, 2024
Accepted October 22, 2024

This work is devoted to edge coupling of optical fibres with waveguides of Si_3N_4-based photonic integrated circuits. At the edge coupling splicing of single-mode optical fibre with high numerical aperture fibre was utilised to reduce the mode field diameter of optical fibre, and for photonic integrated circuit, a field mode converter based on inverse linear taper was employ. The inverse linear taper is a trapezoidal prism which is in contact with a wider part the waveguide and narrowing to $0.3\,\mu$m to the ends of the crystal of the photonic integrated circuit, the height of the trapezium lying at the base of this prism is $300\,\mu$m. Experimentally demonstrated the possibility to reduce the coupling loss to 0.7 dB per edge.

Keywords: Single-mode fibre, high numerical aperture fibre, inverse linear taper, photonic integrated circuit, edge coupling.

DOI: 10.61011/EOS.2024.10.60061.7024-24

Introduction

The size of electronic integrated circuits is gradually decreasing and reaching its physical limit, while the demand for high-speed data processing continues to increase. This limit may only be circumvented by introducing devices that utilize different data processing mechanisms. One possible solution is the use of photons both for data transmission and for data processing. In this context, photonic integrated circuits (PICs) with their high speed and low power consumption provide a real opportunity for further development [1]. Silicon photonics has made great strides in the past decade and is tentatively close to actual application in telecommunications, data transmission, medical technology, security, detection, quantum simulation [2], machine learning [3], and quantum computing [4]. The main driving force behind silicon photonics is the potential to construct a compact and highly integrated system with low cost and high sensitivity. The list of available photonic elements already includes one-dimensional and two-dimensional grating couplers, broadband edge connectors, strip and rectangular waveguides, splitters, ring resonators, electrooptical modulators, etc. [5].

Modern PICs may operate at wavelengths within a wide spectral transparency window (specifically, Si_3N_4 covers the range from visible (~ 400 nm) to infrared ($> 2.5\,\mu$m) wavelengths [6]). Traditional silicon oxide, SiO_2, and silicon, Si, PICs feature a strong refraction index contrast, which leads to miniaturization of devices and, consequently, greater manufacturing complexity [7]. Therefore, waveguides with a core of Si_3N_4 and a SiO_2 cladding, which have a less profound difference between refraction indices, are used in the present study. The resulting device dimensions increase, but manufacturing tolerances also increase. These materials provide an opportunity to fabricate waveguides with transmission losses from 0.3 to 1.0 dB/cm within the spectral range from 400 to 2350 nm [8]. Since PICs are used most often in fiber lines operating at the telecommunication wavelength of the IR range (1550 nm), further analysis is performed for this wavelength.

The primary components of transmission losses are fiber–PIC coupling losses and losses in waveguide matching with various PIC components, such as connectors, sources, and detectors. The most significant contribution is produced by IR radiation coupling losses at the PIC input. A reduction in these losses should help raise the data throughput to levels comparable to the throughput of bulk optical technology [9]. The core diameter of the SMF28 single-mode fiber, which is the basis of modern telecommunications, is several times greater than the PIC waveguide width. Therefore, the mode field diameters (MFDs) of the fiber and the waveguide, which characterize the distribution of the light field within them, differ significantly. The closer the fiber MFD is to the waveguide MFD, the better is the mode matching and the lower is the IR input loss. Therefore, in order to reduce the input loss, one needs to reduce the fiber MFD either by lensing the optical fiber tip or by splicing SMF28 with an ultra-high numerical aperture (UHNA) fiber.

The first method is very intricate, which translates into large MFD variations from one fiber to the other. The second method is technologically simpler and, consequently, more convenient in both scientific research and subsequent commercial production. In addition to reducing the MFD inside a fiber, one may also narrow the MFD directly in a PIC waveguide by installing special integrated optical coupling elements (specifically, edge tapers (trapezoidal prisms)) to achieve the highest matching efficiency. Edge coupling of IR radiation has an advantage over other techniques in its high efficiency and broadband matching; this is the reason why this method was chosen in the present study.

The study is focused on the issue of reduction of fiber–PIC coupling losses for IR radiation through the use of electromagnetic field mode converters, SMF28 fibers spliced with UHNA3, and waveguide sections tapering towards the end facets of the PIC chip (inverse linear tapers). The structure, the process of fabrication, and transmission losses of a fiber mode converter are detailed in Section 1. We managed to reduce average SMF28–UHNA3 splicing losses to a level below 1 dB. In Section 2, the edge coupling method is described in brief and the choice of an inverse linear taper is substantiated; in Section 3, the PIC structure and fabrication are characterized; and in Section 4, the procedure of polishing of PIC end facets with a relative transmission loss variance of 7.9% is discussed. Section 5 is focused on the method for measurement of transmission losses of the PIC with the SMF28 fiber spliced with UHNA3, and the obtained results are analyzed in Section 6.

1. Fiber mode converter

In the present study, first the SMF28 single-mode fiber with a lensed tip and then SMF28 spliced with a high-aperture fiber are used as a fiber mode converter. An optical fiber consists of a core with a higher refraction index and a reflective cladding with a slightly lower refraction index. Layers of protective varnish and coating are always added in production, since fiber is a very fragile material. Owing to the effect of total internal reflection, a beam entering the core of a fiber from its end at an angle greater than the critical one is reflected from the cladding and continues to propagate along the fiber. When the propagation of an electromagnetic wave in a fiber is characterized mathematically, the beam has a Gaussian profile. This profile corresponds to the fundamental TEM00 mode and follows intensity distribution formula

$$I(r) = I_0 \exp\left(\frac{2D^2}{MFD^2}\right),$$

where parameter MFD is the beam diameter at which the light intensity decreases by a factor of e^2 and I_0 is the intensity at the spot center at $D = 0$ [10]. The SMF28 optical fiber has a core $8.2\,\mu$m in diameter made of SiO_2 with the addition of germanium and a reflective cladding $125 \pm 0.7\,\mu$m in diameter made of SiO_2; the effective refraction index is 1.47. The mode field diameter for a wavelength of $1.55\,\mu$m is $10.4 \pm 0.5\,\mu$m. Numerical aperture NA is the ratio of wavelength to the core diameter of a fiber and assumes a value of 0.14 [11]. Since the mode field diameter of SMF28 is significantly larger than the cross-sectional area of a single-mode waveguide [12], the MFD of the fiber should be reduced either by lensing or by installing fiber mode converters.

Table 1. Matching efficiency of two lensed fibers

Fiber numbers	Losses, dB
1 and 2	6.7 ± 1.1
3 and 4	15.8 ± 0.2

Table 2. Key fusion splicing parameters for Fujikura FSM-40S

Discharge power, W	Distance, μm	Overlap, μm	Splicing time, ms
20	15	10	18000

A commercial lensed fiber was the first one to be used in our experiments on edge coupling of radiation from single-mode fiber into a PIC. This lensed fiber was machined from SMF28 in such a manner that its tip was a conical lens. The lensed fiber has a focal point with the smallest mode field diameter; at this point, the MFD was within the $2.5 - 3\,\mu$m range. Transmission losses of the lensed fiber are presented in Table 1. The process of measuring the transmission losses of two optical fibers is similar to the process of measuring the transmission losses of an optical fiber and a PIC waveguide and is detailed below in Section 5. The presented data reveal pronounced parameter variations in fibers that underwent the same processing sequence. The production of lensed fiber is a highly complex process. This has a profound effect on the fiber quality and is an obstacle to research that is not focused on specific methods for reducing the MFD inside a fiber; therefore, an alternative method was used.

This is the technique of splicing SMF28 with UHNA, which is a fiber mode converter. UHNA3 was used. This fiber has a core $1.8\,\mu$m in diameter, $MFD = 4.1 \pm 0.3\,\mu$m at a wavelength of $1.55\,\mu$m, and $NA = 0.35$ [13]. It was spliced with SMF28 in a specially tailored process; the optimum parameters of splicing performed using a Fujikura FSM-40S [14] fusion splicer, which were set in the present study, are listed in Table 2. The ends (4.7 cm in length) of SMF28 and UHNA3 fibers were preprocessed with a Fujikura SS03 stripper to remove the protective coating and varnish and treated with isopropyl alcohol to remove residual glue from the sheath and dust particles. The fibers were then cleaved to a length of 4ċm using a High Precision Cleaver V11 to ensure that their end faces are orthogonal to the cores. Following this, SMF28 and UHNA3 fibers are introduced into a Fujikura FSM-40S fusion splicer. When the splicing process is complete, one obtains an SMF28 fiber with a 4-cm-long UHNA3 tip (SMF28_UHNA3 structure). Another SMF28 fiber is then stripped, treated with isopropyl alcohol, and cleaved. This SMF28 fiber

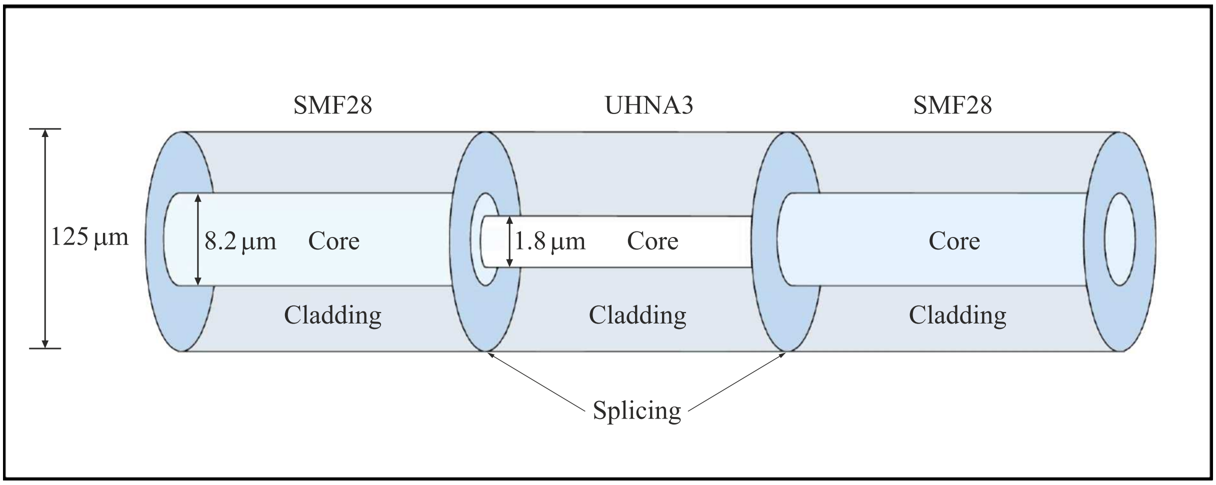

Figure 1. Structure of the composite SMF28_UHNA3_SMF28 fiber.

Table 3. Transmission losses of SMF28_UHNA3 and UHNA3_SMF28

Fiber numbers	Losses, dB
1 and 6	0.5 ± 0.1
2 and 7	0.6 ± 0.1
3 and 8	1.8 ± 0.1
4 and 9	1.2 ± 0.2
5 and 10	0.9 ± 0.1

Table 4. Average transmission losses in matching of two lensed fibers and two SMF28 spliced with UHNA3

Fiber type	Losses, dB
Lensed fiber	11.2 ± 4.2
UHNA3	1 ± 0.3

and the SMF28_UHNA3 structure are introduced into the fusion splicer. The end result is a fiber with two AC/APC connectors at the ends (for connection to a laser and a power meter) and a middle section that is stripped of the protective sheath and glue and consists of SMF28, UHNA3, and SMF28 fibers. This part, the SMF28_UHNA3_SMF28 structure, is shown in Fig. 1. This composite fiber was then cleaved in the middle of UHNA3 to obtain two pieces of SMF28 spliced with UHNA3, which are hereinafter referred to as SMF28_UHNA3 (fiber at the IR radiation input into the PIC waveguide taper) and UHNA3_SMF28 (fiber at the IR radiation output from the PIC waveguide taper). The results of transmission loss measurements for spliced fibers SMF28_UHNA3 and SMF28_UHNA3 matched end-to-end are presented in Table 3.

Table 4 presents the results of measurement of the average transmission losses for different optical fibers. Comparing the transmission losses of two lensed fibers and two fiber mode converters, one sees clearly that significantly lower levels of loss and test data variance are achieved when SMF28_UHNA3 and UHNA3_SMF28 are matched. As was already noted, lensed fibers are characterized by high manufacturing tolerances, which translate into large differences in MFD between the two studied fibers and contribute to an increase in transmission losses. Therefore, SMF28 spliced with UHNA3 was used in further experiments.

2. Inverse linear taper

The matching losses between an optical fiber and the PIC waveguide may be minimized not only by reducing the MFD inside the fiber, but also by fitting the PIC with special integrated optical elements. These elements may be divided into two groups according to the connection method: matching with a grating coupling element and with edge tapers. Grating coupling elements have a number of advantages, such as small dimensions, possibility of testing at the wafer level, and high positioning accuracy; however, they also have significant disadvantages, which include low matching efficiency (usually below 3 dB) and narrow bandwidth. In contrast, edge tapers are characterized by high matching efficiency and wide bandwidth and are polarization-independent, but are also fairly large, provide low positioning accuracy, and impose strict requirements as to the quality of preparation of PIC end facets [1]. Since edge tapers allow one to achieve higher matching efficiency than grating coupling elements, we opted for edge coupling. When a fiber is matched to a waveguide via edge coupling, their ends are connected so that their cores become coaxial, allowing the fiber mode (core diameter, $8.2\,\mu$m) to be transformed smoothly into the waveguide mode (waveguide

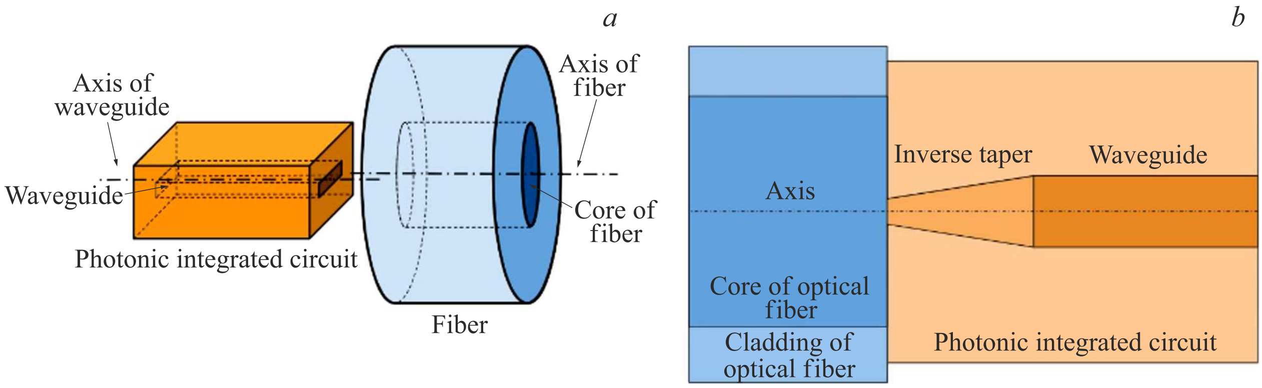

Figure 2. The fiber core and the waveguide are not drawn to scale (the fiber is significantly larger than the waveguide). (*a*) Edge coupling diagram; (*b*) following alignment, the tip of the inverse linear taper is coaxial with the tip of the UHNA3 fiber.

width, 1.3 μm). The edge coupling diagram is shown in Fig. 2.

Edge tapers (trapezoidal prisms) are crucial to fiber–waveguide matching in edge coupling. Many types of such tapers differing in shape and fabrication technology are known. An inverse taper is, as opposed to a direct one, a waveguide that tapers (instead of expanding) towards the PIC end facets. The tip of an inverse taper has a small area compared to the propagation mode of the optical fiber (300×330 nm), and only a part of radiation from this fiber is picked up by the taper. However, as the taper expands, the mode narrows and becomes close in size to the waveguide one, and the closer in size the waveguide and taper-narrowed modes are, the lower are the matching losses (Fig. 2, *b*) [15].

Inverse tapers are characterized by such parameters as matching efficiency, physical dimensions, and accuracy of fiber positioning [16]. The physical dimensions, which factor into the resulting device size, determine the degree of integration, the technological complexity of fabrication, and the possibility of fitting a PIC together with a fiber into a single package for the convenience of data input, processing, and output. Compact dimensions help increase the degree of integration and reduce manufacturing costs. Single-taper edge tapers, which are the easiest to manufacture, are distinguished by high positioning accuracy. It is important to note that radiation propagates in a taper by virtue of distribution of transverse waves of electric and magnetic fields along the width and the thickness of a waveguide, respectively; in order to reduce the dependence on polarization, optical waveguides should be fabricated with square cross sections [17,18]. It is also worth noting that, since single-mode waveguides are considered here, such feature as adiabaticity (propagation of the fundamental mode along the waveguide without transformation into higher-order modes and excitation of other modes) is required of them [19]. A taper may be made adiabatic by increasing its length of the taper to 300 μm. A large number of different types of inverse edge tapers are currently known. The main ones are discussed below.

The first one is a prism with its width increasing from the end to the waveguide. The width may increase gradually in steps with a linear dependence on the waveguide length [20], parabolically, or exponentially [21]. The main advantage of such tapers is the relative simplicity of fabrication of a mask for electron-beam lithography and subsequent manufacture; however, the produced structures are fairly large in size and provide moderate matching efficiencies (no worse than -2 dB).

The next type (multi-tip taper) is a combination of several tapers of the first type [22]. Radiation is introduced into a waveguide through the tips of several tapers arranged in a row, and wide parts of these tapers then merge into a single common taper. A multi-tip taper has a higher matching efficiency (approximately -1.5 dB) and lower required positioning accuracy, but is harder to manufacture.

Edge tapers of the third type feature a diffraction grating; these are linear inverse tapers with a variable refraction index in the direction of radiation propagation [23]. Compared to previous types, such tapers offer strict adiabaticity, are more compact (no larger than 40 μm), and have a bandwidth of about 100 nm at the wavelength of 1550 nm. They are also notable for their high matching efficiencies, -0.75 dB. These tapers are produced via electron-beam lithography, but the manufacturing process is significantly longer than the one typical of the models discussed earlier and requires a larger number of processing tools.

Other taper types, such as edge tapers with several auxiliary waveguides on top [24], multilayer edge tapers (cascade tapers) with the refraction index decreasing gradually from the upper taper to the lower one [25], edge tapers with an overlayer with a lower refraction index [26], edge tapers with their thickness and width varying in the direction of radiation propagation [27], and edge tapers with a cantilever [28], are also available. The matching efficiency of all these structures is no worse than 1 dB, but the processes of their production necessarily feature too

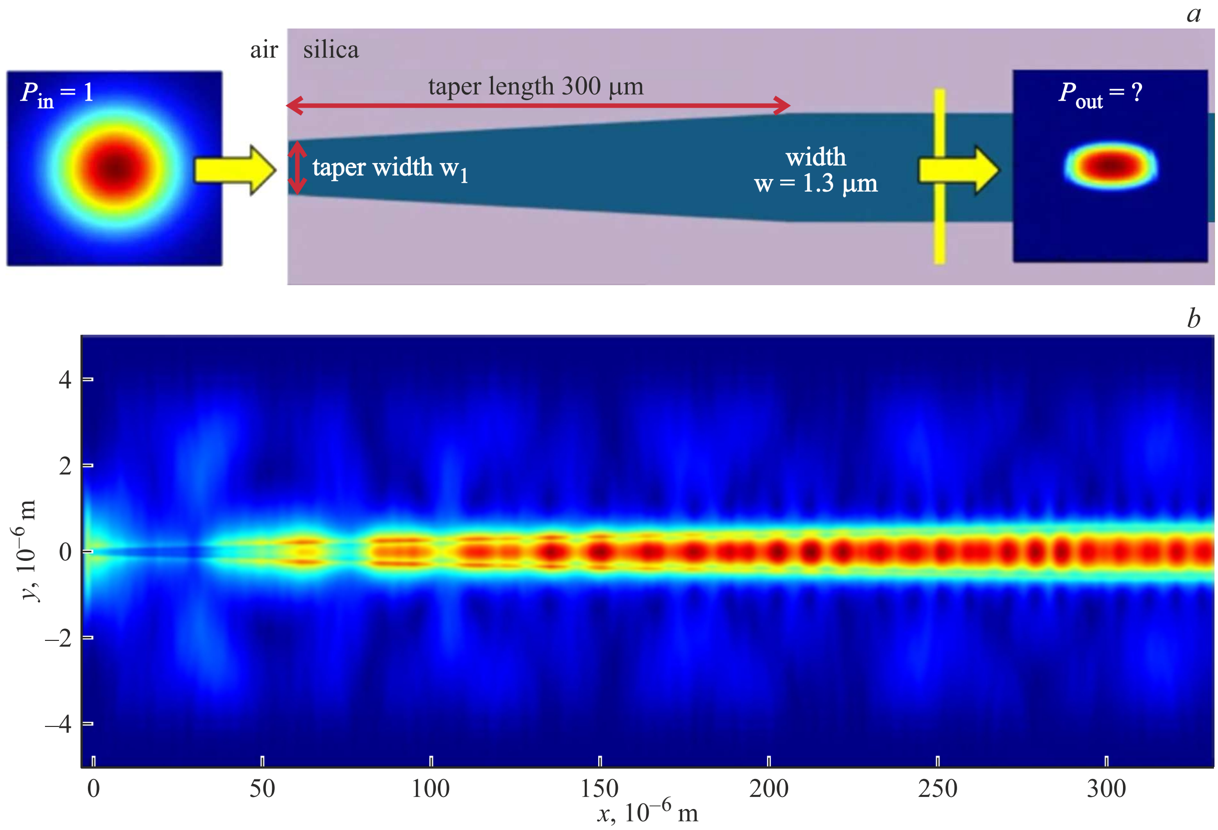

Figure 3. (*a*) Profile of the electric field amplitude of the waveguide at the input and output of IR radiation in the taper [15]; (*b*) propagation of the mode in an inverse linear taper.

many steps to be practical at the current technological level, hindering further commercialization [1].

The present study is aimed at testing the capabilities of current electron-beam lithography technology by calculating the average transmission losses per 1 mm; therefore, the inverse linear taper, which is the easiest to manufacture, was chosen.

3. PIC structure and fabrication technology

The first step toward fabricating waveguides with inverse linear tapers is modeling in the Ansys Lumerical environment (Fig. 3). This modeling involves the determination of geometric dimensions of the structure (waveguide, substrate, and cap layer) and the corresponding materials. It is crucial to set a correct cross-sectional area, since a waveguide too narrow or too wide may inhibit the propagation of the fundamental mode or admit higher-order modes. The modeling domain then needs to be specified: divided into segments and furnished with boundary conditions (only the transverse electric mode is considered). The direction of propagation of the radiation source, which has the form of a Gaussian beam with $MFD = 3.2 - 4.8\,\mu$m and a wavelength of $1.55\,\mu$m, is determined at the next step. The frequency-domain field and power monitor (along the radiation propagation axis) and the mode expansion monitor are then used to model the propagation of radiation in the taper and the waveguide and model the MFD profile at the taper output. After this, the geometric parameters of the inverse linear taper and the waveguide are varied iteratively to calculate the maximum possible theoretical matching efficiency. This efficiency was found to be -0.97 dB; the geometric parameters of the inverse linear taper and the waveguide are shown in Fig. 4.

Next, we used the Python3 GDShelpers library to create template files for lithography. A mask for electron lithography for samples Nos. 1 and 2 with arrays of nine waveguides with the same geometric parameters and lengths of 5 and 7 mm, respectively, was prepared in this environment. Test structures were made from a three-layer Si 500 μm / SiO_2 2.6 μm / Si_3N_4 0.33 μm substrate. A buffer layer with a width of 4 μm was formed in the positive resist around the waveguide via electron-beam lithography. The exposed resist was then developed and washed away. Si_3N_4 was removed in open windows using plasma chemistry methods to form a waveguide of the required geometry. The resulting structure was coated with a layer of silicon oxide via electron-beam evaporation; this coating serves both as a protective layer and as a reflective shell for the waveguide on

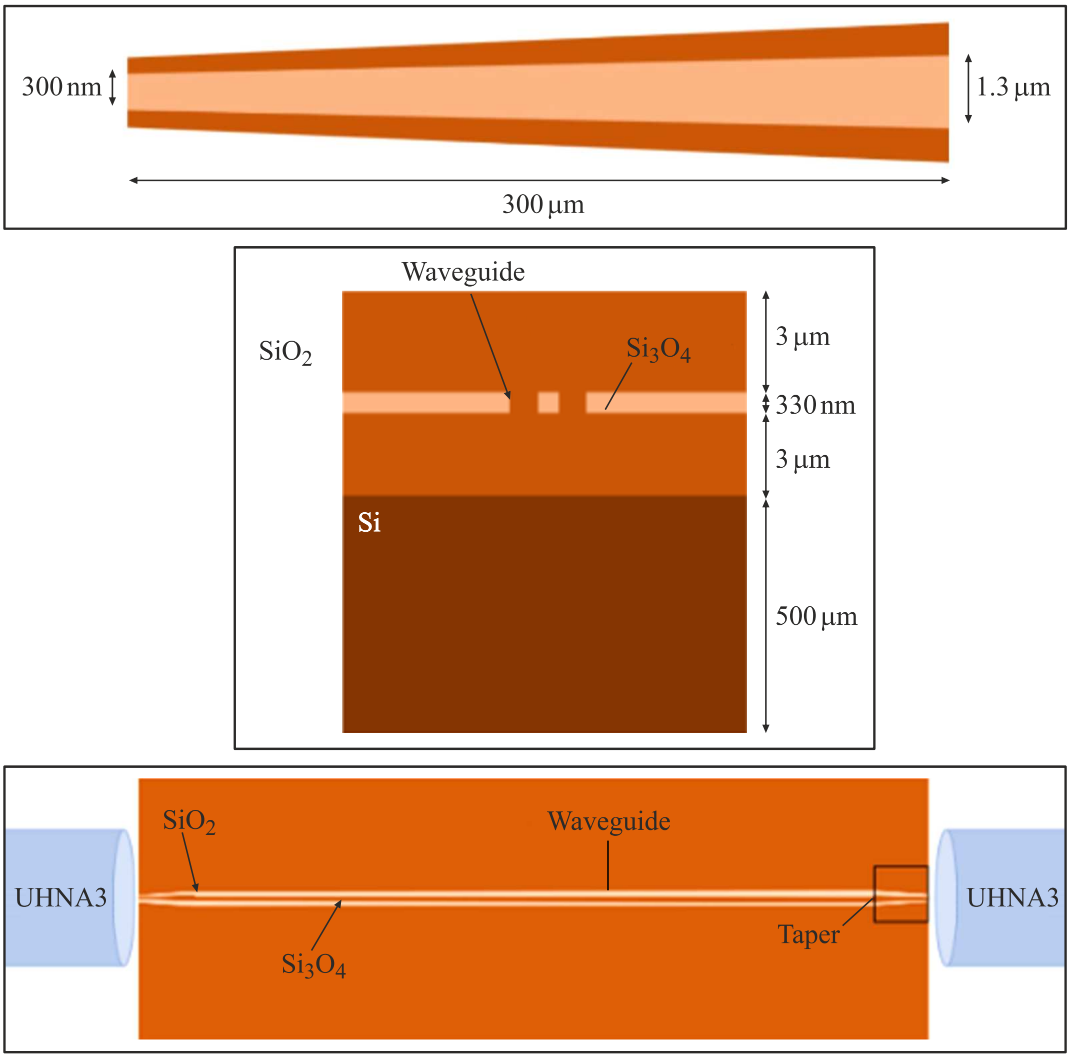

Figure 4. (*a*) Dimensions of the inverse linear taper; (*b*) PIC end facet; and (*c*) part of the structure with one PIC waveguide and optical fibers (nine identical parallel waveguides in each structure).

top. In the present study, each waveguide has the structure shown in Fig. 4, *c*. The photonic integrated circuit prepared for validating the polishing process and calculating the resulting efficiency of matching UHNA3, which is spliced with SMF28, to the PIC featured nine waveguides with inverse linear tapers with identical geometric parameters.

4. Polishing of PIC end facets

Several PIC samples are manufactured together on a silicon wafer, which has a polymer resist material applied to it for protection from damage, and are separated from each other with the use of a diamond scriber of a setup for cutting of various electronic materials. The cut is made at a distance of approximately 100 μm from the taper ends to avoid damaging the PIC waveguides. The end facets of separated samples have high roughness, which is critical for fiber–waveguide matching through edge tapers. Therefore, one needs to polish the end surfaces of the PIC. This polishing was performed by a KrellTech NOVA automatic

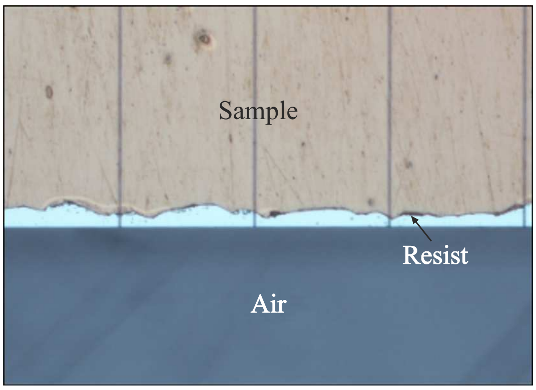

Figure 5. Polished end facet of the PIC sample with waveguides.

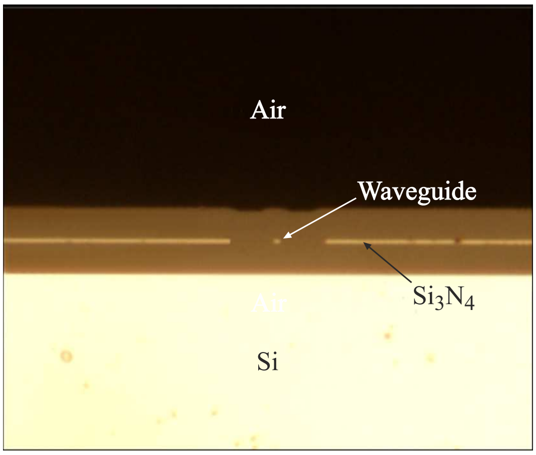

Figure 6. The taper tip is seen clearly on the polished PIC end facet.

optical polishing system. A PIC sample was positioned on a holder and lowered until its end facet touched the film of the polishing disk. Films with SiC (silicon carbide) abrasive particles 3 μm and 0.3 μm in diameter were used in succession. Each film was used for no more than seven minutes (to prevent damage to the PIC end facets from particles formed during polishing), and the samples themselves needed to be rinsed thoroughly in acetone, deionized water, and isopropyl alcohol when films were changed. Polishing with films with 3 μm SiC particles proceeded until the distance to the ends of tapers shortened to $7-10\,\mu$m; the remaining distance to the tapers was traversed with 0.3 μm SiC films. After polishing, the ends of tapers were at the end facets of the PIC (Fig. 5). The second end facet was then polished in a similar manner. Following this, the sample was rinsed in acetone, deionized water, and alcohol preheated to 50°C (for 15 minutes in each liquid) to dissolve the resist and remove any particles remaining after polishing. We managed to achieve a high polishing quality, and the tips of tapers are seen clearly in the optical microscopic image (Fig. 6).

5. Measurement of transmission losses of structure SMF28_UHNA3_PIC_UHNA3_SMF28

The diagram of the measurement setup is shown in Fig. 7 (upper panel). A PLS-1500/9 picosecond optical pulse generator serves as the source of IR radiation with a wavelength of 1550 nm. Infrared radiation enters the fiber that has an APC-polish connector and the prepared SMF28_UHNA3 structure on its opposite ends. Passing through the fiber mode converter, IR radiation exits through the UHNA3 fiber and enters the tip of the PIC taper. The narrowed radiation mode then propagates along the waveguide and enters the second taper. The second taper does, in contrast, expand this mode, since the taper narrows in the direction of propagation of IR radiation. The expanded mode from the taper then enters the UHNA3_SMF28 core and is expanded again by the fiber mode converter. The power of radiation from the UHNA3_SMF28 fiber is measured by a Keysight N7744C power meter; this is the output power (P_{out}) of the SMF28_UHNA3_PIC_UHNA3_SMF28 structure (two fiber mode converters are coupled on both sides via tapers to the PIC waveguide). The input power (P_{in}) is measured by replacing the SMF28_UHNA3_PIC_UHNA3_SMF28 structure with a 0.5-m-long single-mode fiber-optic patch cord with APC polishing on both sides (Fig. 7, bottom panel). Knowing P_{in} and P_{out}, one may calculate the transmission losses of structure SMF28_UHNA3_PIC_UHNA3_SMF28.

As was already noted, the MFD of the UHNA3 fiber and the taper tip width are fairly small (approximately 4 μm and 300 nm, respectively). Therefore, the process of aligning the ends of fibers with the taper ends takes quite a long time. The positioning of the UHNA3 tips relative to the taper tips is adjusted using the 9063-XYZ-PPP-M motorized gothic-arch bearing piezo stages, which are controlled via a personal computer. Goniometer stages needed to nullify the angle between the fiber core axis and the PIC waveguide axis are mounted on these stages. Fibers are secured in Thorlabs HFF003 v-groove fiber holders, which are glued to the goniometer stages. The photonic integrated circuit is fixed on a holder fitted with a micrometer screw, which provides additional control over the angle between the fiber core axis and the PIC waveguide axis. The measurement setup is also fitted with a Moticam 4000 camera needed to verify the coaxial alignment of fiber tips and the waveguides with PIC tapers.

At this adjustment step, the screws of the piezo stages are turned manually. In the course of alignment, one needs to shift the fiber relative to the waveguide in very small increments of 30–600 nm, fitting precisely into the central diffraction maximum observed when 1.55 μm radiation passes through the 1.8 μm core in UHNA3. The SMF28_UHNA3 and UHNA3_SMF28 fibers are first secured in v-grooves and are aligned coaxially with the use of goniometers and piezo stages. The fibers are then brought apart, and the holder with the PIC is positioned between them. In order to reduce radiation input losses, the waveguides should be coaxial with the fiber cores. Thus, the PIC sample, which is monitored via the Moticam 4000 camera, is rotated on the holder fitted with a micrometer screw until the fiber cores and the waveguide become coaxial. The next part of the experiment is carried out on the 9063-XYZ-PPP-M piezo stages controlled by a program run on a personal computer. A pitch of 600 nm is set first, and the SMF28_UHNA3 optical fiber is shifted relative to the waveguide in the Z-, Y-, and X-directions to the position with maximum power. The second UHNA3_SMF28 fiber is then positioned so that the power increases and reaches its new maximum. Following this, the pitch is reduced to 300 nm, and the experiment is repeated with optical fibers SMF28_UHNA3 and UHNA3_SMF28. This step is repeated with a pitch of 150, 60, and 30 nm. When the adjustment

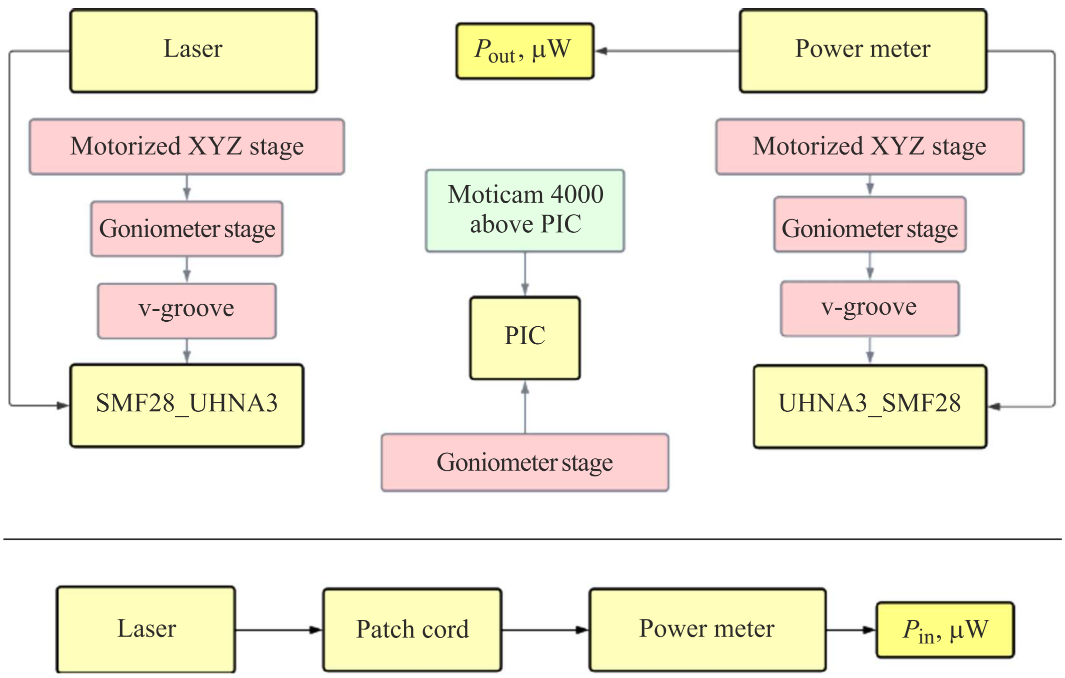

Figure 7. Measurement setup.

Table 5. Transmission losses of the SMF28_UHNA3_PIC_UHNA3_SMF28 structure with a waveguide length of 5 mm

Sample №1	Waveguide length, 5 mm
№waveguide	Losses, dB
2	14.1 ± 0.3
3	15.5 ± 0.4
4	15.8 ± 0.9
6	11.0 ± 0.2
7	12.5 ± 0.2
9	12.3 ± 2.4

Table 6. Transmission losses of the SMF28_UHNA3_PIC_UHNA3_SMF28 structure with a waveguide length of 7 mm

Sample №2	Waveguide length, 7 mm
№waveguide	Losses, dB
1	17.5 ± 0.1
2	15.0 ± 0.1
3	16.9 ± 0.7
4	16.6 ± 0.5
6	16.2 ± 0.2
7	17.8 ± 0.3

process is complete, optical fibers SMF28_UHNA3 and UHNA3_SMF28 become coaxial with the waveguide, and the ends of tapers and fibers are aligned. This is the position in which the output power is always at its maximum. The maximum Pout value is measured by Keysight N7744C.

6. Results

This section is focused on the calculation of transmission losses of the SMF28_UHNA3_PIC_UHNA3_SMF28 structure with 5- and 7-mm-long waveguides, average transmission losses per 1 mm, and the efficiency of matching the PIC to two SMF28 optical fibers spliced with UHNA3.

The transmission losses are calculated as

$$dB = 10 \log\left(\frac{P_{in}}{P_{out}}\right), \tag{1}$$

The transmission losses of the SMF28_UHNA3_PIC_UHNA3_SMF28 structures with waveguides 5 and 7 mm in length are presented in Tables 5 and 6, respectively. These losses were measured five times for each waveguide. The technique of polishing the PIC end facets has been tested for the first time and optimized in the present study (Section 4). Since sample No. 1 was the first to be polished, its surface roughness is higher than that of sample No. 2, and the variance of transmission loss values corresponding to different waveguides is more significant.

Table 7. Transmission losses per 1 mm of waveguide length

Average losses for waveguides with a length of 7 mm, dB	Average losses for waveguides with a length of 5 mm, dB	Average transmission losses, dB/mm
16.4 ± 1.3	12.1 ± 1.0	2.1

The relative variance of transmission losses for samples Nos. 2 and 1 was 7.9% and 8.7%, respectively. It should also be noted that the fiber and the PIC cap layer are made of SiO_2, which is a very fragile material. Therefore, the transmission losses increase in the course of experiments due to the emergence of chipping defects on the ends of fibers and the PIC layer. Comparing Tables 5 and 6, one finds large transmission losses per 1 mm for waveguides with a length of 5 and 7 mm; Table 7 presents the average transmission losses per 1 mm of Si_3N_4 waveguide length.

The technology of fusion splicing of SMF28 and UHNA3 fibers with relatively low losses was optimized in the course of experiments; the average loss value was 1 dB per splice. With losses per unit length of the Si_3N_4 waveguide taken into account, the achieved efficiency of matching one fiber to one PIC end facet is approximately -0.7 dB. The formula for its calculation is presented below, where L_w are the average losses per waveguide, L_{sp} are the average fiber splicing losses, and L_{mm} are the average losses per 1 mm of waveguide length:

$$(L_w - L_{sp} - L_{mm})/2. \qquad (2)$$

Conclusion

The study was focused on the measurement of efficiency of matching a waveguide with an inverse linear taper to the SMF28 optical fiber spliced with UHNA3. The key challenge in calculating matching efficiency is to identify the underlying mechanisms affecting losses and suppress them, thus increasing the data throughput required for further implementation in quantum technology. Two PIC structures with waveguide lengths of 5 and 7 mm were fabricated for this purpose. Each PIC consisted of nine Si_3N_4 waveguides. All of them were fitted with two inverse linear tapers for matching to optical fibers through which IR radiation is introduced into the waveguide and output from it. These fibers were prepared by splicing the SMF28 fiber with UHNA3. This structure had low average splicing losses (below 1 dB). The used splicing method is relatively new and was refined in the course of experiments. The average transmission losses for two waveguide lengths were measured and calculated. The obtained values revealed large transmission losses of the waveguide, which reached 2.1 dB/mm. The resulting matching efficiency was calculated to be as high as -0.7 dB.

Funding

This study was supported by the Russian Science Foundation, grant № 23-12-00187, https://www.rscf.ru/project/23-12-00187/.

Conflict of interest

The authors declare that they have no conflict of interest.

References

[1] X. Mu, S. Wu, L. Cheng, H.Y. Fu. Appl. Sci., **10** (4), 1538 (2020). DOI: 10.3390/app10041538

[2] C. Sparrow, E.Martín-López, N. Maraviglia, A. Neville, C. Harrold, J. Carolan, Y.N. Joglekar, T. Hashimoto, N. Matsuda, J.L. O'Brien, D.P. Tew, A. Laing. Nature, **557**, 660–667 (2018). DOI: 10.1038/s41586-018-0152-9

[3] G.R. Steinbrecher, J.P. Olson, D. Englund, J. Carolan. npj Quantum Inf 5, 60 (2019). DOI: 10.1038/s41534-019-0174-7

[4] H. Choi, M. Pant, S. Guha, D. Englund. npj Quantum Inf 5, 104 (2019). DOI: 10.1038/s41534-019-0215-2

[5] T.L. Koch, U. Koren. IEEE J. Quant. Electron., **27** (3), 641–653 (1991). DOI: 10.1109/3.81373

[6] D.J. Blumenthal, R. Heideman, D. Geuzebroek, A. Leinse, C. Roeloffzen. Proc. IEEE, **106** (12), 2209–2231 (2018). DOI: 10.1109/JPROC.2018.2861576

[7] C.R. Doerr. Frontiers Phys., **3**, 37 (2015). DOI: 10.3389/fphy.2015.00037

[8] M.A. Tran, D. Huang, T. Komljenovic, J. Peters, A. Malik, J. Bowers. Appl. Sci., **8** (7), 1139 (2018). DOI: 10.3390/app8071139

[9] Hui Wang, Jian Qin, Xing Ding, Ming-Cheng Chen, Si Chen, Xiang You, Yu-Ming He, Xiao Jiang, L. You, Z. Wang, C. Schneider, Jelmer J. Renema, Sven Höfling, Chao-Yang Lu, Jian-Wei Pan. Phys. Rev. Lett., **123** (25), 250503 (2019). DOI: 10.1103/PhysRevLett.123.250503

[10] *Lazernye tekhnologii* [Electronic source]. URL: https://online.mephi.ru/courses/new_technologies/laser/data/lecture/9/p5.html

[11] *Opticheskoe volokno Corning SMF-28 Ultra. Opisanie izdeliya* [Electronic source]. URL: https://www.ssd.ru/upload/iblock/214/smf_28ultra.pdf

[12] N.V. Nikonorov, S.M. Shandarov *Volnovodnaya fotonika. Uchebnoe posobie, kurs lektsii.* (ITMO, SPb, 2008) (in Russian).

[13] *Ultra-High NA Single-Mode Fibers* [Electronic source]. URL: https://www.coherent.com/resources/datasheet/components-and-accessories/specialty-optical-fibers/uhna3_spec_202011122126.pdf

[14] S. Preble. *UHNA Fiber — Efficient Coupling to Silicon Waveguides. Application Note NuAPP-3* [Electronic source]. URL: https://www.coherent.com/resources/application-note/components-and-accessories/specialty-optical-fibers/uhna-fiber-efficient-coupling-to-silicon-waveguides.pdf

[15] S. Chuang. *Physics of Photonic Devices* (John Wiley & Sons, NJ, 2009).

[16] C. Kopp, S. Bernabé, B.B. Bakir, J.M. Fedeli, R. Orobtchouk, F. Schrank, H. Porte, L. Zimmermann. IEEE J. Sel. Top. Quant., **17** (3), 498–509 (2011). DOI: 10.1109/JSTQE.2010.2071855

[17] G.T. Reed, A.P. Knights. *Silicon Photonics: An Introduction* (John Wiley & Sons, NJ, 2004).
[18] Y. Ding, J. Xu, F. Da Ros, B. Huang, H. Ou, C. Peucheret. Opt. Express, **21** (8), 10376–10382 (2013). DOI: 10.1364/OE.21.010376
[19] T. Ramadan, R.M. Osgood. J. Lightwave Technol., **16** (2), 277 (1998).
[20] P. Suchoski, R. Ramaswamy. IEEE J. Sel. Top. Quant., **23** (2), 205–211 (1987). DOI: 10.1109/JQE.1987.1073307
[21] S.J. Hettrick, J. Wang, C. Li, J.S. Wilkinson, D.P. Shepherd. J. Lightwave Technol. **22** (3), 845–849 (2004). DOI: 10.1109/JLT.2004.824548
[22] X. Mu, S. Wu, L. Cheng, X. Tu, H. Fu. *OSA Technical Digest (Frontiers in Optics + Laser Science APS/DLS)* (Optica Publishing Group, Washington, 2019). DOI: 10.1364/FIO.2019.JTu3A.66
[23] P. Cheben, D.X. Xu, S. Janz, A. Densmore. Opt. Express, **14** (11), 4695–4702 (2006). DOI: 10.1364/OE.14.004695
[24] M.J. Picard, C. Latrasse, C. Larouche, Y. Painchaud, M. Poulin, F. Pelletier, M. Guy. Proc. SPIE OPTO, **9752**, 132–138 (2016). DOI: 10.1117/12.2208629
[25] J.K. Doylend, A.P. Knights. IEEE J. Selected Topics in Quant. Electron., **12** (6), 1363–1370 (2006). DOI: 10.1109/JSTQE.2006.884409
[26] J.-M. Lee, D.-J. Kim, H. Ahn, S.-H. Park, G. Kim. J. Lightwave Technol., **25** (8), 2236–2243 (2007). DOI: 10.1109/JLT.2007.899792
[27] M. Fritze, J. Knecht, C. Bozler, C. Keast, J. Fijol, S. Jacobson, P. Keating, J. LeBlanc, E. Fike, B. Kessler, M. Frish, C. Manolatou. J. Vacuum Sci. Technol. B, **21** (6), 2897–2902 (2003). DOI: 10.1116/1.1625967
[28] Q. Fang, T.S. Liow, J. Song, C. Tan, M. Yu, G. Lo, Kwong, D.L. Opt. Express, **18** (8), 7763–7769 (2010). DOI: 10.1364/OE.18.007763

Translated by D.Safin